Kinetics of homogeneous and heterogeneous reactions in the reductive aminolysis of glucose with dimethylamine

Jeroen Poissonnier[a], Michiel Pelckmans[b], Frederik Van Waes[c], Kristof Moonen[c], Bert F. Sels[b], Joris W. Thybaut[a,*], Guy B. Marin[a]

[a] Ghent University, Laboratory for Chemical Technology, Technologiepark 914, B-9052 Gent, Belgium
[b] KU Leuven, Department M2S, Celestijnenlaan 200F, B-3001 Leuven, Belgium
[c] Eastman Chemical Company, Technologiepark 21, B-9000 Gent, Belgium

ABSTRACT

The reductive aminolysis of glucose with dimethylamine (DMA) as aminating agent has been investigated experimentally as well as via kinetic model construction. A fed-batch reactor configuration was used at following conditions: temperatures ranging between 383 K–398 K, total pressures from 6.0 MPa to 7.5 MPa, an overall catalyst to glucose ratio of 9–31 g_{cat} mol^{-1}, an overall DMA to glucose ratio of 12–24 mol mol^{-1} and an overall hydrogen to glucose ratio of 5–10 mol mol^{-1}. Such a reactor configuration, combined with a controlled feeding rate of the sugar, allowed to significantly avoid degradation reactions. The main desired products, i.e., dimethylaminoethanol (DMAE) and tetramethylethylenediamine (TMEDA), were obtained after amination followed by retro-aldol cleavage with maximum selectivity, amounting up to 15% and 60% respectively. Retro-aldol cleavage after amination proceeds at lower temperatures, evidenced by an activation energy of 60 kJ mol^{-1}, than without amination, where activation energies amounting to 140 kJ mol^{-1} have been reported. A higher catalyst to glucose ratio leads to more parallel side products such as *N,N*-dimethylglucamine and 4-dimethylamino-1,2,3-butanetriol. The effects of temperature and catalyst to glucose ratio were much more pronounced than that of the total pressure or the ratio of the aminating agent to glucose. The developed kinetic model is based on the most prominent homogeneous bulk phase and heterogeneously catalyzed reactions and accounts quantitatively for degradation reactions. A statistically and physically significant model which could satisfactorily reproduce the experimental observations, was thus obtained.

1. Introduction

Fuels and chemicals production predominantly rely on fossil resources. With the perspective of a more sustainable society and industry, renewable feedstocks are gaining more and more popularity in the production of the same or at least similar fuels and chemicals. Therefore a global shift in attention from conventional resources towards biomass can be observed [1,2].

Subsequent generations have been defined with respect to biomass, the first one comprising biodiesel and bioethanol from sources such as sugar cane and corn starch, while the second generation stems from lignocellulosic feedstock [3]. Although first generation biomass has been commercialized, it is still under heavy debate as it enters in direct competition with food production [4,5]. Therefore, second generation biomass such as (waste) lignocellulose, which consists of lignin, hemicellulose and cellulose, has become more prominent as a renewable source for biofuels and chemicals [5]. A wide variety of valorization routes has already been explored for (ligno)cellulosic biomass, e.g., via the production of sorbitol, glucose and hydroxymethylfurfural as platform molecules [6–8]. These components are subsequently converted into value added compounds such as propylene glycol, ethylene glycol, ethanol, etc. [9–11]

In the present work we particularly focus on the production of acyclic alkylamines and aminoalcohols from cellulosic biomass. Especially the formation of the latter from biomass is promising, since the alcohol function is already present in the starting product. In alternative biomass based processes such as gasification or bioethylene formation these functionalities are lost and have eventually to be reintroduced [12,13]. Chemicals containing nitrogen functions, such as aminomethylfurans, are already being produced from renewable resources [14]. E.g., the biodegradable and nontoxic insecticide 5-aminolevulinic acid and the surfactant 5-methyl-*N*-alkyl-2-pyrrolidone can be formed with high atom efficiency [15]. The production of the latter involves levulinic acid production from carbohydrates with formic acid

Notation

Roman letters

a_j	Activity of component j, $mol\,m_L^{-3}$
CN_j	Number of carbon atoms of component j originating from a glucose feed molecule
C_t	Total concentration of active sites, $mol\,kg_{cat}^{-1}$
$E_{a,i}$	Activation energy of reaction i, $kJ\,mol^{-1}$
F	F-value for global significance of the regression
f_j	Fugacity of component j, Pa
F_j	Molar flow rate of component j, $mol\,s^{-1}$
$K_{ads,j}$	Adsorption equilibrium coefficient of component j, $m_L^3\,mol^{-1}$
k_i	Rate coefficient of reaction i, reaction dependent
K_j^{VL}	Vapor-liquid equilibrium coefficient of component j
n_{exp}	Number of experiments
n_j	Molar amount of component j, mol
p	Pressure, MPa
R	Universal gas constant, $J\,mol^{-1}\,K^{-1}$
r_i	Extensive reaction rate of reaction i, $mol\,s^{-1}$
R_j	Net production rate of component j, $mol\,s^{-1}$
S_j	Selectivity of component j originating from glucose, $mol\,mol^{-1}$
t	Batch time, s
T	Temperature, K
t_0	Glucose feed time, s
T_{ave}	Average temperature, K
V	Reactor volume, m_r^3
W_{cat}	Catalyst mass, g_{cat}

w_j	Weight factor corresponding to response j
X	Glucose conversion, $mol\,mol^{-1}$
x_j	Liquid phase molar fraction of component j
y_j	Gas phase molar fraction of component j

Greek letters

ε	Liquid fraction in the reactor, $m_L^3\,m_r^{-3}$
φ_j	Activity coefficient of component j
θ_j	Fractional site coverage of component j

Symbols

◊	Active acid site
*	Active metal site

Subscripts

◊	Adsorbed species on an acid site
*	Adsorbed species on a metal site
T_{ave}	Average temperature

Superscripts

^	Modeled
°	Susceptible to degradation
0	Initial
L	Liquid
V	Vapor

as byproduct. The levulinic acid is subsequently aminated and hydrogenated in-situ over a ruthenium catalyst. The required hydrogen can be obtained from decomposition of the formic acid, rendering the byproduct very useful in this process [15]. Several biobased amine production pathways and applications were recently summarized and well described by Froidevaux et al. [16]. Of particular interest for this work are amines produced from carbohydrates and their derivatives. E.g. 1,4-butanediamine and 2-pyrollidone are already being produced from glucose derivatives on industrial scale [17]. In addition, several macromolecules, such as polyamides, are synthesized partially or totally biobased [18].

The reductive amination of isomaltulose with *n*-dodecylamine leads to products with excellent surfactant properties. A kinetic model has been proposed for this reaction making use of a simplified reaction network. Apart from the desired conversion steps, degradation reactions of the Maillard type, among others, significantly complicate the kinetic analysis. A catalyst screening showed that palladium is the best performing catalyst for a reductive amination and that the amount of degradation products can be limited by decreasing the starting material concentration, temperature and pH [19,20]. Despite these degradation reactions, the experimentally measured concentrations over a palladium catalyst could be reproduced in a satisfactory manner using the mathematical model [21].

In the present work, glucose is considered as a model compound for cellulosic biomass. The formation of ethanolamine and diaminoethane has already been witnessed during the reductive amination of glucose with ammonia at temperatures above 373 K and total pressures above 12 MPa on a Ni catalyst, indicating the occurrence of a so-called aminolysis reaction [22]. A kinetic model is constructed for the reductive aminolysis of glucose. The knowledge of previous mechanistic and kinetic studies on the reductive amination of alcohols and aldehydes is thus expanded with an experimental and mathematical description of the reductive aminolysis of sugars [23–25]. The aminolysis is

mechanistically substantially different from the one studied before for esters and thioesters [26,27]. Dimethylamine (DMA) has been selected as the aminating agent to limit the complexity of the reaction network. Alternative aminating agents such as ammonia would yield α-amino carbonyl compounds when reacting with sugars, which, in turn, cyclize to pyrazines and piperazines, after hydrogenation [28,29]. DMA offers an adequate balance between complexity of the occurring reaction network and ability to assess the biomass valorization kinetics in a fundamental manner.

2. Procedures

2.1. Experimental

In a preliminary set of batch experiments in which all reactants as well as the catalyst were introduced to the reactor before heating was started, low desired product yields were obtained. This behavior was attributed to an uncontrolled temperature rise as a consequence of the exothermicity of the hydrogenolysis reaction. Correspondingly, degradation occurred to a significant extent, as evidenced by the typical brown color of the product mixture. In order to mitigate these issues, a fed-batch reactor configuration was employed in which glucose was only admitted to the reactor after having reached the desired operating conditions. In this manner, the actual glucose concentration is kept sufficiently low such that temperature excursions and, hence, degradation reactions are maximally avoided.

Three-phase kinetic experiments, where a liquid reactant is treated under a hydrogen gas atmosphere on a solid catalyst have been performed in a 1 l ($1 \times 10^{-3}\,m^3$) fed-batch reactor. The commercially available Ni KL6504K-P (60% Ni/SiO_2) catalyst was acquired from CRI Catalyst Company. DMA was provided by Eastman Chemical Company, and all other chemicals were used as available from commercial suppliers without further pretreatment or purification. The reactor content

is continuously mixed using a stirrer at 300 RPM. The liquid phase is sampled through a tube submerged in the reactor liquid. The operating conditions are reported in Table 1.

Each experiment starts with the loading of the catalyst suspended in water into the reactor vessel. Next, the stirrer is started and the desired amount of DMA is charged to the reactor. DMA, present in a separate vessel as a liquid under its own vapor pressure, is pressurized using helium and introduced into the reactor, leading to a pressure increase of ± 0.2 MPa. Subsequently, the vessel is heated up to the reaction temperature, resulting in an additional pressure increase of ± 2 MPa. When the desired temperature is reached the set pressure is built up using hydrogen. An internal cooling circuit ensures that this temperature can be maintained during reaction. Finally, the experiment is started, i.e. t = 0 s, and the glucose solution is pumped into the reactor by means of a HPLC pump. The amount of glucose fed is such that a finite time t_0, ranging from 1200 to 5100 s, is required for this. The hydrogen consumption throughout the experiment is monitored by continuously adding fresh hydrogen to maintain the total reactor pressure. ± 5400 s after t_0 the hydrogen consumption stops, indicating that no further conversion is taking place in the reactor and that only final reaction products remain. Starting at t_0 samples are taken every 900 s. These samples are analyzed by means of gas chromatography. Two independent analyses are performed to determine the composition of both the lighter and heavier end of the components contained in the liquid. The light end typically comprises DMAE and TMEDA, while the heavy end typically consists of *N,N*-dimethylglucamine and 4-di-methylamino-1,2,3-butanetriol. The latter are subject to acetylation, as used for alcohol and amino groups in drug analysis prior to analysis [30]. The carbon balance, based on the carbon atoms from the reactant glucose, could be closed for at least 75% in every experiment, with a single exception for the experiment where the catalyst to glucose ratio was the lowest and degradation reactions were most prominent.

The absence of possible mass transfer limitations was verified by calculating the corresponding criteria for the most severe conditions. The most crucial heterogeneously catalyzed reaction is the hydro-genation of the C_2 enamine (see below) and the Carberry number for gas-liquid and liquid-solid mass transfer was calculated using the rate of this step in a conservative way, i.e. where all glucose is converted instantaneously to three C_2 enamine species. The Carberry number corresponding to H_2 mass transfer from gas to liquid amounts to 0.028 and the Carberry number corresponding to liquid-solid mass transfer, which is more critical for the enamine than for H_2, amounts to 0.035, which both are well below the limit of 0.05 [31,32]. Possible heat transfer effects were investigated by the Mears criteria [33]. Internal and external temperature gradients amount to 0.004 and 0.04 K respectively, which are sufficiently smaller than the criterion leading to a 5% deviation of the observed reaction rate. Temperature control on the reactor scale is the most critical in this process. The maximal thermal power produced by reaction exothermicity is 145 W, which can be removed using the internal cooling circuit, such that isothermicity on the reactor scale can be ensured.

2.2. Definitions

The experimental results are quantified in terms of glucose conversion and product selectivities. The former is defined as the fraction of the reactant consumed by reaction:

$$X = \frac{n_{glucose}^0 - n_{glucose}}{n_{glucose}^0} \quad [\text{mol} \quad \text{mol}^{-1}]$$

(1)

The selectivity towards product j is calculated using Eq. (2), where CN_j represents the number of carbon atoms originating from the glucose feed.

$$S_j = \frac{CN_j(n_j - n_j^0)}{6(n_{glucose}^0 - n_{glucose})} \quad [\text{mol} \quad \text{mol}^{-1}]$$

(2)

In Eq. (2) n_j^0 typically equals 0 as no products are co-fed.

2.3. Modeling

2.3.1. Fed-batch reactor model equations

The molar amount of each component j present in a fed-batch reactor can be determined at every time t by solving the differential Eq. (3) representing the mass balance for this component j.

$$\frac{dn_j(t)}{dt} = R_j(t) + F_j(t) \quad [\text{mol} \quad \text{s}^{-1}]$$

(3)

For the surface species the pseudo steady state approximation is applied:

$$R_j = 0 \quad [\text{mol s}^{-1}]$$

(4)

In Eq. (3) the flow rate $F_j(t)$ represents the feed term which is only different from zero for glucose dissolved in water and hydrogen. The net rate of formation R_j of each component j can be determined from the rate expressions shown in Eqs. (16)–(24), see below. The integration of this set of equations constituting the pseudo-homogeneous reactor model is performed using an open-source code, DASPK, a differential-algebraic equation solver available from Netlib [34].

Vapor-liquid equilibrium is assumed to be instantaneously established. The latter is achieved when the Gibbs free energy of the gas and the liquid phase are equal. This condition can also be expressed as the equality of the corresponding chemical potentials or the corresponding vapor and liquid phase fugacities, provided that identical reference states have been selected for the gas and the liquid phase respectively, see Eq. (5) [35].

$$f_j^L = f_j^V \quad [\text{MPa}]$$

(5)

The latter can be rewritten in terms of activity coefficients as:

$$x_j \varphi_j^L = y_j \varphi_j^V$$

(6)

The composition can then be obtained from the expression of the vapor-liquid equilibrium coefficient, Eq. (7).

$$K_j^{VL} = \frac{y_j}{x_j} = \frac{\varphi_j^L}{\varphi_j^V}$$

(7)

The mixture volumes required for calculating the fugacity coefficients are determined using the Predictive Soave-Redlich-Kwong (PSRK) equation of state [36]. The activity coefficients were estimated using the UNIFAC model [37].

2.3.2. Parameter estimation

The forward rate and the adsorption equilibrium coefficients are expressed according to the Arrhenius and van't Hoff relationship, in

Table 1
Summary of the experimental conditions of the fed-batch reductive aminolysis of glucose with DMA

Property	Symbol	Value	Units
Catalyst mass	W_{cat}	2.9–7.4	g_{cat}
Temperature	T	383–398	K
Pressure	p	6.0–7.5	MPa
Glucose feed[a]	$n_{glucose}^0$	0.2–0.4	Mol
Hydrogen to glucose ratio	$n_{H2}/n_{glucose}^0$	4.7–9.6	mol mol^{-1}
DMA to glucose ratio	$n_{DMA}/n_{glucose}^0$	11.9–23.6	mol mol^{-1}
Glucose concentration		500	$g_{glucose}/l_{H2O}$

[a] $F_{glucose}$ varies between 5×10^{-5} and 3×10^{-4} mol s^{-1}, n^0 is the total amount of glucose fed.

reparametrized form. This reparametrization is performed to reduce the statistical correlation between the activation energy/reaction enthalpy and the pre-exponential factor. It involves the rewriting of the coefficient as a function of the rate or equilibrium coefficient at the mean temperature $k_{T,ave}/K_{T,ave}$ and the activation energy E_a/reaction enthalpy ΔH_R as in Eq. (8) [38,39]. A similar expression can be written down for the equilibrium coefficients.

$$k_i = k_{T,ave,i} \exp\left(-\frac{E_{a,i}}{R}\left(\frac{1}{T} - \frac{1}{T_{ave}}\right)\right) \quad (8)$$

The reverse rate coefficients are determined from the corresponding forward rate coefficients and the thermodynamic equilibrium coefficients.

22 adjustable model parameters, stemming from 4 adsorption equilibrium coefficients and 7 rate coefficients, each determined by two parameters to describe their temperature dependence as in Eq. (8), are estimated based on the minimization of the weighted sum of squares of the residuals between the experimentally determined composition and the model calculated composition as in Eq. (9).

$$SSQ = \sum_{k=1}^{n_{exp}} \sum_{j=1}^{n_{resp}} w_j (n_{k,j} - \hat{n}_{k,j})^2 \xrightarrow{k_{T,ave}, E_a} Min \quad (9)$$

The weights w_j tune the dependence of the SSQ on the various responses, such that good estimates can be obtained for most, if not all, of the parameters allowing to adequately reproduce the glucose conversion and main product selectivities. Parameter estimation is performed in a stage-wise manner. In the first stage an in-house developed software implementation of the Rosenbrock method is used to approximate the solution [40]. The resulting parameter estimates are subsequently fine-tuned using the Levenberg-Marquardt algorithm, as available in ODRPACK [41]. Statistical testing was performed to verify the kinetic model performance. The individual significance of the model parameters was verified by confirming that zero is not included in the individual 95% confidence interval. The global significance of the regression is verified with an *F* test. The regression is deemed to be globally significant when the *F* value exceeds the tabulated *F* value, meaning that the regression sum of squares significantly exceeds the residual sum of squares divided by the corresponding degrees of freedom [39].

3. Effects of reaction conditions

A simplified reaction network representing the key intermediates and reaction products is shown in Fig. 1. Smaller molecules are formed from glucose via a retro-aldol cleavage. Each molecule shown on the left side in Fig. 1 leads to the aminated product on the right. *N,N*-Di-methylglucamine and 4-dimethylamino-1,2,3-butanetriol, i.e., the 2 top right compounds in the network are the undesired end products, while the 2 bottom right compounds, i.e., DMAE and TMEDA, are the desired ones.

The effects of varying temperature, total pressure, catalyst to glucose ratio, aminating agent to glucose ratio, and feed rate of the glucose solution have been investigated to assess their impact on the reductive aminolysis of glucose with DMA. Due to the complex chemistry involved, the experimental observations reflect combined effects of varying operating conditions rather than clearly isolated effects of a varying condition on the product spectrum. Nevertheless, quite relevant information could be retrieved from this experimentation which proved to be useful for the model assessment.

3.1. Temperature

Higher temperatures have shown to enhance the glucose conversion. This is evident from the measured glucose concentrations at 383 K in the samples after t_0 whereas at 398 K glucose concentrations are

always zero in these samples. This indicates that the initial condensation between the sugar and the DMA has a high activation energy. Higher temperatures also increase the selectivity towards TMEDA, while that towards *N,N*-dimethylglucamine is significantly suppressed. This is an indication that the retro-aldol cleavage has a higher activation energy than the hydrogenation step, see also Fig. 2.

3.2. Total pressure

The total pressure effect is not very pronounced. The selectivity towards TMEDA slightly decreases at a lower total pressure as the hydrogen solubility is correspondingly decreased. The importance of degradation reactions is increased at lower total pressures as more DMA is present in the gas phase and correspondingly the liquid phase glucose concentration is higher.

3.3. Catalyst to glucose ratio

When the catalyst to glucose ratio is increased the selectivity towards *N,N*-dimethylglucamine and 4-dimethylamino-1,2,3-butanetriol is significantly enhanced. The selectivity towards TMEDA correspondingly decreases. The selectivity towards degradation products is also decreased. The latter indicates that the catalyst to glucose ratio is a good measure for the hydrogenation capacity. A high catalyst to glucose ratio results in longer chain hydrogenation products such as *N,N*-di-methylglucamine while a lower ratio favors the retro-aldol cleavage products. The latter can, however, not be exploited to the lower limit because of the degradation reactions that become more and more important in the absence of the catalyst.

In the investigated range of operating conditions, higher desired product selectivities were obtained with higher catalyst to glucose ratios, amounting to up to maximum 15% and 60% for DMAE and TMEDA respectively.
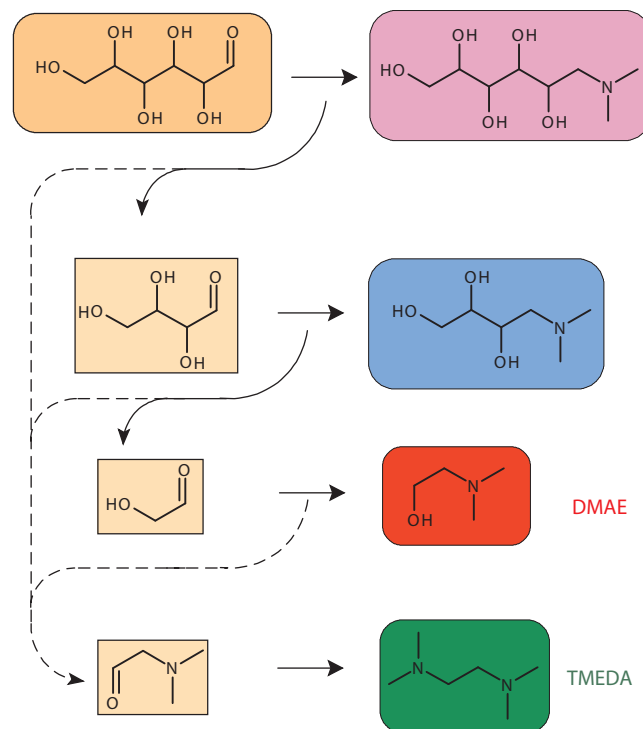

Fig. 1. Simplified representation of the reaction network involved in the reductive aminolysis of glucose with dimethylamine. Molecules with the same reactive moieties as the glucose feed molecule that are formed are shown below the feed molecule, the corresponding aminated product of each of the molecules is shown on the right. The end products from top to bottom: *N,N*-dimethylglucamine, 4-dimethylamino-1,2,3-butanetriol, dimethylaminoethanol (DMAE) and tetramethylethylenediamine (TMEDA).
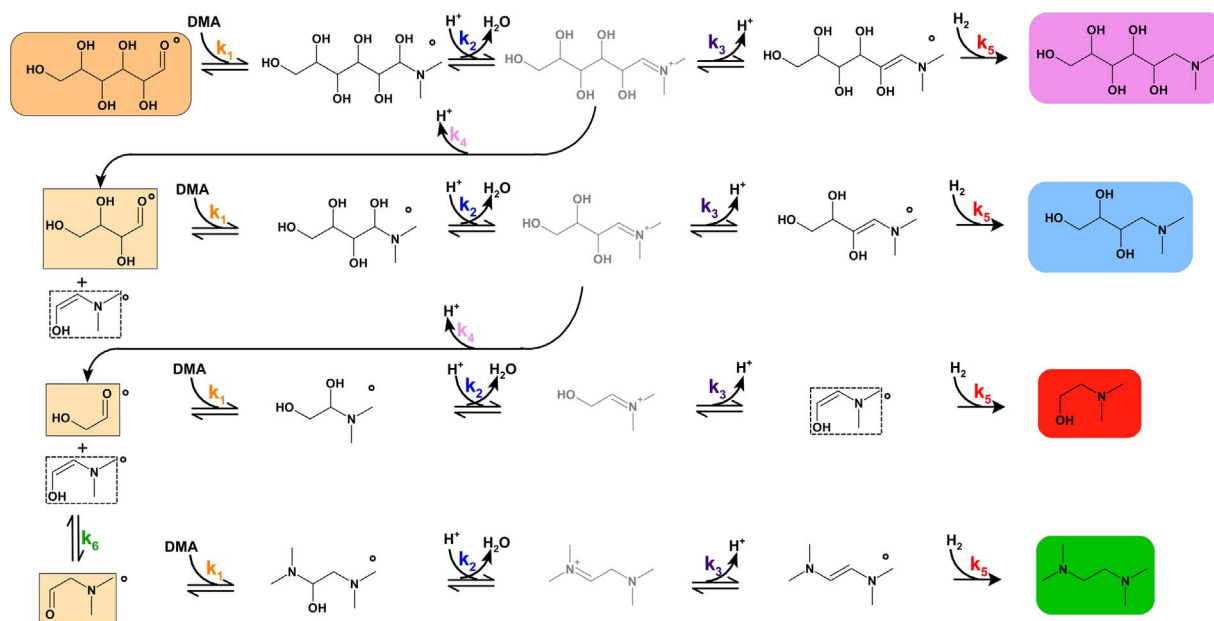
Fig. 2. Reaction network involved in the reductive aminolysis of glucose with dimethylamine. The molecules shown in full lined boxes are similar to the feed molecule and undergo the same sequence of reactions. The molecule shown in the dashed lined boxes is always the same but can be formed in multiple ways. The molecules marked by an ° are susceptible to degradation. The species indicated in grey are reactive intermediates which will only be present in small quantities.

3.4. DMA to glucose ratio

Increasing the ratio of the aminating agent, e.g. DMA, to glucose enhances the selectivity towards TMEDA. The latter is immediately evident from the reaction network as a higher initial DMA to glucose ratio will ensure a higher DMA availability at a similar glucose conversion and, hence, a higher probability for the amination reactions to occur "further" in the reaction network. A complete conversion of glucose to TMEDA requires six DMA molecules per glucose molecule while only three are necessary for DMAE formation, and one for both *N,N*-dimethylglucamine and 4-dimethylamino-1,2,3-butanetriol.

3.5. Glucose feed rate

A lower feed rate of the glucose solution into the reactor results in a higher selectivity towards *N,N*-dimethylglucamine and 4-dimethyla-mino-1,2,3-butanetriol. The glucose feed rate effect is equivalent to that of increasing the catalyst to glucose ratio, because by decreasing the glucose feed rate the actual catalyst to glucose ratio is higher.

4. Kinetic model development

4.1. Reaction network

The more elaborate glucose aminolysis reaction network, employing DMA as aminating agent, that has been used in the kinetic model development is presented in Fig. 2. It comprises the essential reaction steps to understand the formation of the desired products.

This reaction network entails both heterogeneously catalyzed as well as homogeneous bulk phase reactions. Experiments without heterogeneous catalyst as well as DFT calculations provided further inspiration for this reaction mechanism [42,43]. In the experiment without heterogeneous catalyst 100% glucose conversion to, almost exclusively, degradation products was obtained. This indicated that the degradation reactions are homogeneous. The condensation of glucose with DMA (r_1) to the hemi-aminal is a bulk phase reaction, which is homogeneously catalyzed by DMA. Among the subsequent reactions, i.e., the dehydration of the latter hemi-aminal to an iminium ion (r_2), the rearrangement of the iminium ion to the enamine (r_3), the retro-

aldol cleavage of the iminium ion (r_4) and the hydrogenation of the enamine (r_5) at least one step benefits from the presence of the heterogeneous catalyst. The PSSA can be applied to the very reactive iminium ion (dotted-line box in Fig. 2). Alternative structures of this ion, e.g., intramolecularly generated, complementary to the one obtained after heterogeneous protonation and dehydration as proposed, here may exist [42,43]. The impact of the exact structure of the iminium ion is limited for the practical (mathematical) purposes of the present modeling effort.

The catalyst is considered to host two types of catalytic sites where the different compounds can adsorb and react. Hydrogen adsorbs on one type of sites, i.e., the metallic sites, responsible for the hydrogenation reactions (r_5) while the carbon species adsorb on acid sites. The keto-enol tautomerism (r_6) is again a homogeneously catalyzed bulk phase reaction. The reactive moieties in the molecules obtained after the retro-aldol cleavage are identical to those in the feed molecule glucose and, hence, the same sequence of elementary steps is considered in their further conversion. These molecules are indicated by the full line boxes in Fig. 2. The C_2 enamine split off via the retro-aldol cleavage (dashed-line box in Fig. 2) is the same in each of these steps. It is denoted as a C_2 enamine, since only two of its carbon atoms originate from the glucose feed molecule. Apart from the desired reactions involved in the reductive aminolysis degradation reactions occur which convert glucose to unspecified byproducts. These degradation reactions, such as thermal decomposition and the Maillard reaction, occur via a rather complex mechanism [44]. Given the diversity of considerations that can be made about such reactions, they are accounted for in a simplified manner in the reaction network considered in the present work, i.e., they are considered to be first order in the reactant since these reactions typically start by a decomposition reaction, without specifying which degradation products are exactly formed. This results in a manageable reaction network where the degradation reactions, consuming sugars, hemi-aminals and enamines, each of them being marked with a circle, are modeled as global reactions (r_7, not shown in Fig. 2).

4.2. Rate equations

The extensive reaction rates, rather than intensive reaction rates

because the former can be directly related to the reactor volume for both homogeneous and heterogeneously catalyzed reactions, can be calculated in correspondence with the reaction network as proposed in Fig. 2. The reactions have been grouped into reaction families with the same model parameters, in this way the number of parameters to estimate remains reasonable. For each reaction family the corresponding rate equation is shown for its first occurrence in the network.

The component adsorption is described making use of 4 adsorption coefficients. 3 of them, i.e., $K_{ads,C6}$, $K_{ads,C4}$, $K_{ads,C2}$, relate to glucose and derived species. For these species, the number of carbon atoms originating from the feed glucose appears to be a good measure for their overall size and, hence, their degree of interaction with the catalyst. Hence, a single adsorption coefficient is used for species with the same number of carbon atoms originating from the feed glucose. These components are assumed to adsorb on the acid sites and are contained in the corresponding site balance. The fourth and last adsorption coefficient is the one for dissociative hydrogen adsorption, $K_{ads,H2}$. A separate site balance on the metal sites is constructed for hydrogen. A sufficient metal dispersion is assumed for this catalyst such that hydrogen can easily spill over to the carbon species on the acid sites to hydrogenate them.

The surface coverages can be determined from the adsorption steps which are considered quasi-equilibrated. For the species adsorbing on the acid sites, see below, the surface coverages can be calculated according to Eq. (10):

$$\theta_{\diamond,i} = K_{ads,i} a_i \theta_\diamond \tag{10}$$

For hydrogen, adsorbing on the metal sites the surface coverage is calculated as in Eq. (11):

$$\theta_{*,H} = \sqrt{K_{ads,H2} a_{H_2}}\, \theta_* \tag{11}$$

The site balances are shown in Eqs. (12) and (13):

$$\theta_\diamond + \sum_{i=C_2,C_4,C_6} (\theta_{\diamond,hemi,i} + \theta_{\diamond,im,i} + \theta_{\diamond,enam,i}) = 1 \tag{12}$$

$$\theta_* + \theta_{*,H} = 1 \tag{13}$$

For the heterogeneously catalyzed steps several parameters are lumped together in a composite rate coefficient, see Eqs. (14) and (15):

$$k_i = k_i' C_{t,\diamond} \quad i = 2, 3, 4 \tag{14}$$

$$k_5 = k_5' C_{t,\diamond} C_{t,*}^2 \tag{15}$$

with $C_{t,\diamond}$ and $C_{t,*}$ the total concentration of active acid and metal sites respectively.

The condensation step is a reversible homogeneously catalyzed bulk phase reaction as shown in Eq. (16). This second order dependence originates from the double role DMA plays, i.e., that of a homogeneous catalyst and of a reactant.

$$r_1 = (k_1 a_{DMA}^2 a_{glucose} - k_{-1} a_{DMA} a_{hemi,C_6}) \varepsilon V \quad [\text{mol} \quad \text{s}^{-1}] \tag{16}$$

The second reaction is the reversible dehydration of the hemi-aminal to the iminium ion. The calculation of this rate requires the knowledge of the iminium ion surface species concentration. The pseudo-steady state approximation as shown in Eq. (17), leads upon solution to the iminium ion concentration, Eq. (18).

$$\frac{d\theta_{\diamond,imC_6^+}}{dt} = \big(k_2 \theta_{\diamond,hemiC_6} - k_{-2}\theta_{\diamond,imC_6^+} a_{H_2O} - k_3 \theta_{\diamond,imC_6^+} + k_{-3}\theta_{\diamond,enamC_6}$$
$$- k_4 \theta_{\diamond,imC_6^+}\big) W_{cat} \cong 0 \quad [\text{s}^{-1}] \tag{17}$$

$$\theta_{\diamond,imC_6^+} = \frac{k_2 \theta_{\diamond,hemiC_6} + k_{-3}\theta_{\diamond,enamC_6}}{k_{-2}a_{H_2O} + k_3 + k_4} \quad (-) \tag{18}$$

The rates of the following steps are presented in Eqs. (19)–(24). The retro-aldol cleavage of the iminium ion is considered irreversible as the formed enamine is more easily converted into DMAE or TMEDA rather

than returning to the highly unstable iminium ion. Also the enamine hydrogenation is considered to be irreversible at the mild temperatures used in the experimental campaign. The validity of this assumption is discussed below.

$$r_2 = (k_2 \theta_{\diamond,hemiC_6} - k_{-2}\theta_{\diamond,imC_6^+} a_{H_2O}) W_{cat} \quad [\text{mol} \quad \text{s}^{-1}] \tag{19}$$

$$r_3 = (k_3 \theta_{\diamond,imC_6^+} + k_{-3}\theta_{\diamond,enamC_6}) W_{cat} \quad [\text{mol} \quad \text{s}^{-1}] \tag{20}$$

$$r_4 = k_4 \theta_{\diamond,imC_6^+} W_{cat} \quad [\text{mol} \quad \text{s}^{-1}] \tag{21}$$

$$r_5 = k_5 \theta_{\diamond,enamC_6} \theta_{*,H}^2 W_{cat} \quad [\text{mol} \quad \text{s}^{-1}] \tag{22}$$

$$r_6 = (k_6 a_{enamC_2} a_{DMA} + k_{-6} a_{C_4H_9NO} a_{DMA}) \varepsilon V \quad [\text{mol} \quad \text{s}^{-1}] \tag{23}$$

$$r_7 = k_7 a_{glucose} \varepsilon V \quad [\text{mol s}^{-1}] \tag{24}$$

The adsorbed species surface fractions as required in Eqs. (17)–(22) can be calculated from the respective adsorption equilibria, see Eqs. (10) and (11). Reaction 6 is a keto-enol tautomerism which is base catalyzed. Hence, the concentration of DMA, the most abundant base in the reaction mixture, is included in this expression for the forward as well as for the reverse rate, see Eq. (23).

4.3. Modeling the reductive aminolysis of glucose with DMA

The estimates for the rate coefficients and the adsorption equilibrium coefficients are presented in Tables 2 and 3 respectively.

It can be seen from Tables 2 and 3 that all parameters are estimated significantly as 0 is not included in any of the individual 95% confidence intervals. The regression is also globally significant with an F value amounting to 160, which sufficiently exceeds the tabulated one of 2.79. Furthermore, no significant correlation exists between the parameter estimates as the maximum binary correlation coefficient is limited to 0.80, i.e., between $K_{Tave,C2}$ and $\Delta H_{ads,H2}$. The model reproduces the data well as can be seen from Fig. 3.

It is also evident from Fig. 3 that the glucose conversion is very fast and more than half of the total amount of glucose fed is already converted at t_0. Shortly after full glucose conversion is achieved the DMAE and TMEDA yields reach their final, plateau values. This confirms that considering irreversibility for the enamine hydrogenation is valid under the applied conditions, particularly no indication for DMAE dehydrogenation was found. Fig. 3-b shows that the model is also capable of reproducing the product spectrum at a lower total pressure, i.e., at conditions where more degradation reactions occur and lower product yields are obtained. The extent of degradation reactions is further enhanced by the combined effect with the lower DMA to glucose ratio. Fig. 3-c shows that the slower conversion of glucose at lower temperatures is reproduced. Furthermore the selectivities towards DMAE and TMEDA are accurately simulated. Finally, the model also manages to correctly simulate the product spectrum at conditions with a lower glucose feed rate, where the actual glucose concentration is thus lower

Table 2
Parameter estimates of the rate coefficients with their 95% confidence intervals obtained after regression of the kinetic model of glucose aminolysis with DMA to the experimental data obtained on a 60% Ni/SiO$_2$ catalyst.

Estimated average rate coefficient			Estimated activation energy (kJ mol^{-1})		
$k_{Tave,1}$	$6.3\ 10^{-10} \pm 4.7\ 10^{-11}$	$m_L^6\,mol^{-2}\,s^{-1}$	$E_{a,1}$	78.1	$\pm\ 7.2$
$k_{Tave,2}$	$2.1\ 10^4 \pm 6.1\ 10^3$	$mol\,kg_{cat}^{-1}\,s^{-1}$	$E_{a,2}$	49.9	$\pm\ 4.9$
$k_{Tave,3}$	$7.0\ 10^{-2} \pm 1.3\ 10^{-2}$	$mol\,kg_{cat}^{-1}\,s^{-1}$	$E_{a,3}$	47.5	$\pm\ 7.9$
$k_{Tave,4}$	$3.9\ 10^{-1} \pm 6.8\ 10^{-2}$	$mol\,kg_{cat}^{-1}\,s^{-1}$	$E_{a,4}$	59.9	$\pm\ 9.9$
$k_{Tave,5}$	$5.0\ 10^1 \pm 7.3$	$mol\,kg_{cat}^{-1}\,s^{-1}$	$E_{a,5}$	8.8	$\pm\ 2.5$
$k_{Tave,6}$	$8.9\ 10^{-4} \pm 1.2\ 10^{-4}$	$m_L^3\,mol^{-1}\,s^{-1}$	$E_{a,6}$	1.6	$\pm\ 0.3$
$k_{Tave,7}$	$2.8\ 10^{-3} \pm 2.2\ 10^{-4}$	s^{-1}	$E_{a,7}$	141.7	$\pm\ 13.0$

Table 3

Parameter estimates of the adsorption equilibrium coefficients with their 95% confidence intervals obtained after regression of the kinetic model of glucose aminolysis with DMA to the experimental data obtained on a 60% Ni/SiO$_2$ catalyst.

Estimated average adsorption coefficient ($m_L^3 \, mol^{-1}$)		Estimated adsorption enthalpy (kJ mol^{-1})	
$K_{Tave,C6}$	$5.7 \, 10^{-5} \pm 1.0 \, 10^{-5}$	$\Delta H_{ads,C6}$	-30.3 ± 9.1
$K_{Tave,C4}$	$6.7 \, 10^{-2} \pm 6.4 \, 10^{-3}$	$\Delta H_{ads,C4}$	-13.7 ± 1.9
$K_{Tave,C2}$	$1.3 \, 10^{-3} \pm 2.8 \, 10^{-4}$	$\Delta H_{ads,C2}$	-26.0 ± 4.6
$K_{Tave,H2}$	$1.1 \pm 3.0 \, 10^{-1}$	$\Delta H_{ads,H2}$	-2.9 ± 0.3

at any time during the experiment. The model performance is shown in Fig. 4 in terms of parity diagrams. The model performs best in simulating the amount of DMAE, see Fig. 4-a, while the amount of TMEDA is also simulated well, see Fig. 4-b. Slight deviations in the model simulated TMEDA amounts can be explained by the modeling of degradation reactions as a single reaction.

The molar amount of the reactant glucose is also well simulated, as shown in Fig. 4-c for the data points at t$_0$ of each experiment. These experimental data points are most remote from the origin. At the other sampling times glucose concentration is almost zero and errors in quantifying/analyzing these amounts are of the same or a larger order of magnitude as the actual concentration. The kinetics for glucose conversion are thus well reproduced. Finally, the model succeeds in simulating the right order of magnitude for formation of *N,N*-dimethylglucamine under the applied fed-batch conditions as seen in Fig. 4-d.

The R^2 values for glucose aminolysis are in the range of 0.7–0.9 for the reactant and the main products, which is very reasonable for the fundamental type of modeling adopted in this work. The side product has a very low R^2 value, which can be expected for a side product which is formed in substantially lower amounts.

5. Discussion

High activation energies for retro-aldol cleavage reactions amounting to 110 kJ mol^{-1} for two β-hydroxy compounds or even to 140 kJ mol^{-1} for glucose, and 80 kJ mol^{-1} for the consecutive smaller chain retro-aldol cleavage, have been reported [45,46]. From Table 2 it can be seen that the activation energy for the retro-aldol cleavage of a C−C bond (E$_{a,4}$) in the present work is significantly lower. The presence of the nitrogen atom next to this C−C bond reduces the retro-aldol cleavage activation energy by up to 80 kJ mol^{-1}. As a result, retro-aldol

cleavage after a preliminary amination proceeds at significantly lower temperatures than required for similar cleavages in the absence of a neighboring N-atom [47]. A possible explanation for such a lower activation energy is situated in the transition state stabilization by electrons donated by the nitrogen function. The higher activation energy for the retro-aldol cleavage (E$_{a,4}$) compared to the iminium ion rearrangement to the enamine (E$_{a,3}$) explains the experimentally observed increase of C$_2$ products DMAE and TMEDA with increasing temperatures at the expense of *N,N*-dimethylglucamine.

In the reductive alkylation of aromatic amines the first reaction step is the condensation of an amine with an aldehyde [48]. The rate coefficient of this reaction amounts to 2×10^{-6} m^3 mol^{-1} s^{-1}. In our work the corresponding parameter k$_1$ amounts to 6×10^{-10} m^6 mol^{-2} s^{-1}. However, because base catalysis is concerned, this parameter value should be corrected for the activity of DMA, which amounts to about 10^4 mol m^{-3}. The corrected k$_1$ value, hence, amounts to 6×10^{-6} m^3 mol^{-1} s^{-1}, which is of the same order of magnitude of the one reported for the reductive alkylation of amines.

Also the activation energy for hydrogenation (E$_{a,5}$) is significantly reduced by the presence of nitrogen heteroatoms. Typical C−C bond hydrogenation activation energies, e.g., for ethylene over Ni catalysts, are in the range from 40 to 45 kJ mol^{-1} [49]. The presence of one or more nitrogen atoms in the chain results in a reduced activation energy for the double bond hydrogenation amounting to only 9 kJ mol^{-1}. In the reductive alkylation of aniline with acetone and the reductive amination of benzaldehyde with ammonia the ratio of the rate coefficient of the hydrogenation reaction to the rate coefficient of the condensation reaction is of the order of magnitude of 10^2–10^3 [50,51]. After correction for the units to allow comparison with this work the ratio k$_5$/k$_1$ amounts to 800.

The activation energy for the degradation reaction was estimated at 140 kJ mol^{-1}, approximately, which is higher than expected for thermal degradation, which has an activation energy of around 115 kJ mol^{-1} [52]. The latter is attributed to other degradation reactions contributing to this global step. This high activation energy, besides high reactant concentrations and long heating times, also partially explains why almost exclusively degradation products were formed during the initial batch experiments with very poor exothermicity control.

The effect of the catalyst to glucose ratio is well simulated. Similar considerations can be made for the glucose feed rate. The model performs well at low feed rates, but extension to the upper limit should be done with caution as the actual glucose concentration enters the region
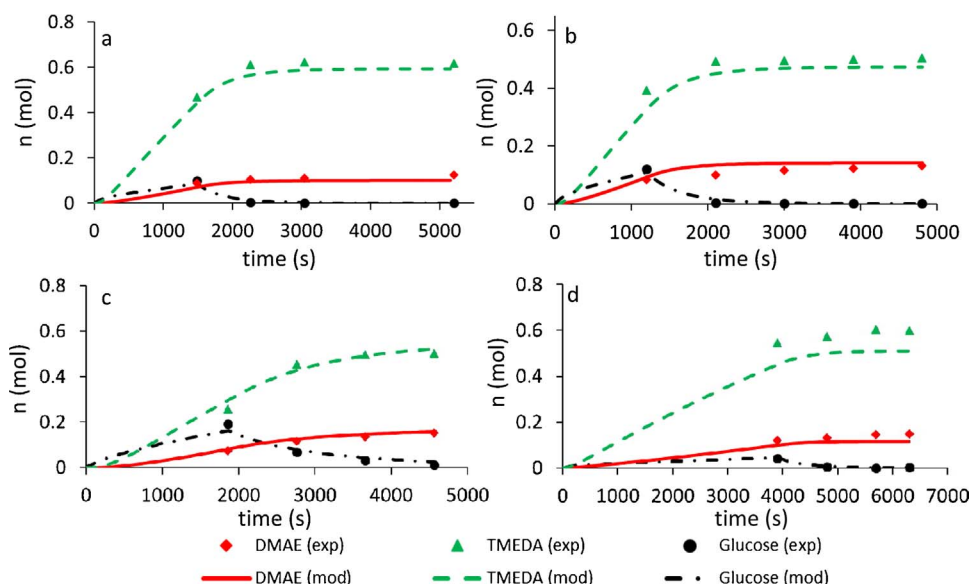
Fig. 3. Molar amounts of DMAE, TMEDA and glucose as a function of the batch time for fed-batch experiments of glucose aminolysis with DMA on a commercial 60% Ni/SiO$_2$ catalyst. At t = 0 s glucose feeding starts up to t$_0$, evidenced by the maximum amount of glucose at the batch time corresponding to the first experimental data point. (a): T = 398 K, $n_{glucose}^0$ = 0.40 mol, p = 7.5 MPa, W$_{cat}$ = 3.6 g, $n_{DMA}/n_{glucose}^0$ = 15.6, t$_0$ = 1484 s. (b): T = 398 K, $n_{glucose}^0$ = 0.40 mol, p = 6.0 MPa, W$_{cat}$ = 4.0 g, $n_{DMA}/n_{glucose}^0$ = 11.9, t$_0$ = 1200 s. (c) T = 383 K, $n_{glucose}^0$ = 0.40 mol, p = 7.5 MPa, W$_{cat}$ = 3.6 g, $n_{DMA}/n_{glucose}^0$ = 12.0, t$_0$ = 1860 s. (d) T = 398 K, $n_{glucose}^0$ = 0.40 mol, p = 7.5 MPa, W$_{cat}$ = 3.6 g, $n_{DMA}/n_{glucose}^0$ = 12.0, t$_0$ = 3900 s. The symbols represent the experimentally observed values while the lines represent the model simulated values using Eq. (3) with the parameters presented in Tables 2 and 3.
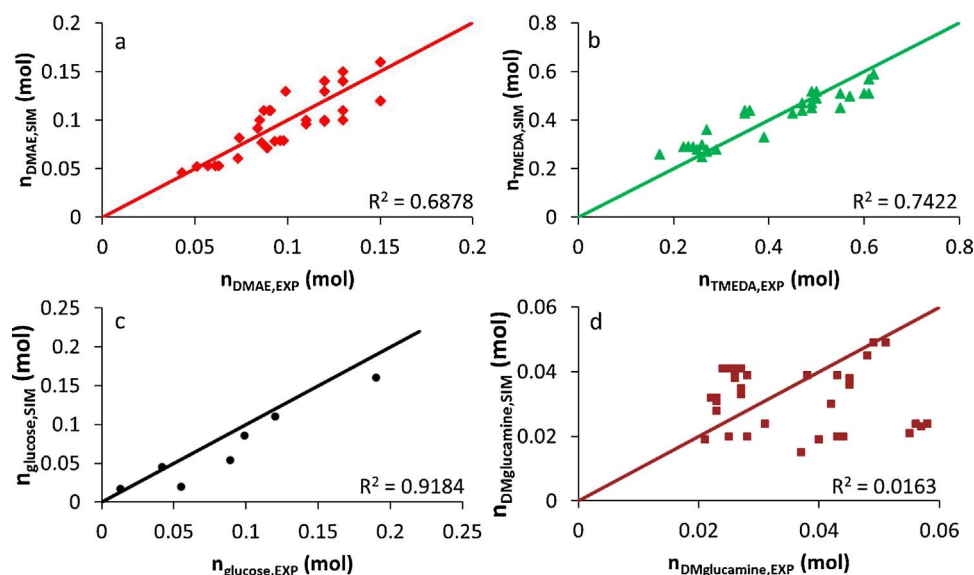
Fig. 4. Parity diagram for the responses of the kinetic model for glucose aminolysis with DMA on a commercial 60% Ni/SiO$_2$ catalyst: molar amount of DMAE (a), molar amount of TMEDA (b), molar amount of glucose (c), molar amount of N,N-dimethylglucamine (d). The model simulated values are obtained from Eq. (3) with the parameters presented in Tables 2 and 3.

where degradation reactions become more pronounced, see also Eq. (24), and, hence, where a more detailed representation of the degradation reactions would be required. The effect of the aminating agent to glucose ratio is simulated slightly more pronounced than experimentally observed.

There is no indication that different rate coefficients should be used within a single reaction family, since the model simulated values can reproduce the experimentally measure results well, see Fig. 3, within the range of operating conditions studied in this work. The developed kinetic model can be used for multi scale simulations to asses which affects would occur when the reductive aminolysis of biomass based glucose is to be performed on a larger scale, where transport phenomena and non-ideal reactor hydrodynamics also potentially contribute to the overall observed behavior [53].

6. Conclusions

A kinetic model has been constructed for the glucose aminolysis with DMA in a fed-batch reactor configuration. The considered reaction network comprises homogeneous bulk phase as well as heterogeneously catalyzed kinetic steps. It allows describing the formation of DMAE and TMEDA as desired products but also N,N-dimethylglucamine and degradation products as side products. The model is able to accurately reproduce the yield of mains products DMAE and TMEDA within the experimentally investigated range of operating conditions, where the effect of the degradation reactions was quantitatively assessed. All model parameters are statistically significant and exhibit a precise physical meaning without being correlated to each other. The incorporation of a nitrogen atom in the carbohydrate chain leads to lower activation energies of both the retro-aldol cleavage and the hydrogenation reaction compared to similar reactions without nitrogen present in the corresponding molecules.

Acknowledgments

References

[1] A. Demirbaş, Biomass resource facilities and biomass conversion processing for fuels and chemicals, Energy Convers. Manage. 42 (2001) 1357–1378.
[2] A.M. Ruppert, K. Weinberg, R. Palkovits, Hydrogenolysis goes bio: from carbohydrates and sugar alcohols to platform chemicals, Angew. Chem. Int. Ed. 51 (2012) 2564–2601.
[3] S.N. Naik, V.V. Goud, P.K. Rout, A.K. Dalai, Production of first and second generation biofuels: a comprehensive review, Renew. Sustain. Energy Rev. 14 (2010) 578–597.
[4] S. Bezergianni, A. Dimitriadis, A. Kalogianni, P.A. Pilavachi, Hydrotreating of waste cooking oil for biodiesel production. Part I: effect of temperature on product yields and heteroatom removal, Bioresour. Technol. 101 (2010) 6651–6656.
[5] R. Deutschmann, R.F. Dekker, From plant biomass to bio-based chemicals: latest developments in xylan research, Biotechnol. Adv. 30 (2012) 1627–1640.
[6] A. Shrotri, A. Tanksale, J.N. Beltramini, H. Gurav, S.V. Chilukuri, Conversion of cellulose to polyols over promoted nickel catalysts, Catal. Sci. Technol. 2 (2012) 1852–1858.
[7] H. Kobayashi, M. Yabushita, T. Komanoya, K. Hara, I. Fujita, A. Fukuoka, High-yielding one-pot synthesis of glucose from cellulose using simple activated carbons and trace hydrochloric acid, ACS Catal. 3 (2013) 581–587.
[8] J.N. Chheda, Y. Roman-Leshkov, J.A. Dumesic, Production of 5-hydroxymethylfurfural and furfural by dehydration of biomass-derived mono- and polysaccharides, Green Chem. 9 (2007) 342–350.
[9] M. Besson, P. Gallezot, C. Pinel, Conversion of biomass into chemicals over metal catalysts, Chem. Rev. 114 (2014) 1827–1870.
[10] J.A. Geboers, S. Van de Vyver, R. Ooms, B.O. de Beeck, P.A. Jacobs, B.F. Sels, Chemocatalytic conversion of cellulose: opportunities, advances and pitfalls, Catal. Sci. Technol. 1 (2011) 714–726.
[11] B. Hahn-Hägerdal, M. Galbe, M.F. Gorwa-Grauslund, G. Lidén, G. Zacchi, Bio-ethanol – the fuel of tomorrow from the residues of today, Trends Biotechnol. 24 (2006) 549–556.
[12] E.S. Lipinsky, Chemicals from biomass: petrochemical substitution options, Science 212 (1981) 1465–1471.
[13] M.H. Bender, Potential conservation of biomass in the production of synthetic organics, Resour. Conserv. Recycl. 30 (2000) 49–58.
[14] A. Cukalovic, C.V. Stevens, Production of biobased HMF derivatives by reductive amination, Green Chem. 12 (2010) 1201–1206.
[15] Y.-B. Huang, J.-J. Dai, X.-J. Deng, Y.-C. Qu, Q.-X. Guo, Y. Fu, Ruthenium-catalyzed conversion of levulinic acid to pyrrolidines by reductive amination, ChemSusChem 4 (2011) 1578–1581.
[16] V. Froidevaux, C. Negrell, S. Caillol, J.-P. Pascault, B. Boutevin, Biobased amines from synthesis to polymers; present and future, Chem. Rev. 116 (2016) 14181–14224.
[17] I. Bechthold, K. Bretz, S. Kabasci, R. Kopitzky, A. Springer, Succinic acid a new platform chemical for biobased polymers from renewable resources, Chem. Eng. Technol. 31 (2008) 647–654.
[18] L. Jasinska, M. Villani, J. Wu, D. van Es, E. Klop, S. Rastogi, C.E. Koning, Novel, fully biobased semicrystalline polyamides, Macromolecules 44 (2011) 3458–3466.
[19] R. Cartarius, T. Krause, H. Vogel, Catalyst development for the reductive amination of isomaltulose, Eng. Life Sci. 3 (2003) 327–333.
[20] R. Cartarius, T. Krause, H. Vogel, Degradable surfactants via heterogeneously catalyzed reductive amination of isomaltulose–examination of catalyst deactivation in a continuous gradient free reaction vessel, Eng. Life Sci. 1 (2001) 55–59.
[21] R. Cartarius, T. Krause, H. Vogel, A kinetic modeling of reductive amination of isomaltulose on a palladium catalyst, Eng. Life Sci. 2 (2002) 53–59.
[22] A. Fischer, T. Mallat, A. Baiker, Amination of diols and polyols to acyclic amines, Catal. Today 37 (1997) 167–189.
[23] A. Baiker, W. Caprez, W.L. Holstein, Catalytic amination of aliphatic alcohols in the gas and liquid phases: kinetics and reaction pathway, Ind. Eng. Chem. Prod. Res. Dev. 22 (1983) 217–225.
[24] A.W. Heinen, J.A. Peters, H. van Bekkum, The reductive amination of benzaldehyde

over Pd/C catalysts: mechanism and effect of carbon modifications on the selectivity, Eur. J. Org. Chem. 2000 (2000) 2501–2506.

[25] S. Gomez, J.A. Peters, T. Maschmeyer, The reductive amination of aldehydes and ketones and the hydrogenation of nitriles: mechanistic aspects and selectivity control, Adv. Synth. Catal. 344 (2002) 1037–1058.

[26] S. Ilieva, B. Galabov, D.G. Musaev, K. Morokuma, H.F. Schaefer, Computational study of the aminolysis of esters. the reaction of methylformate with ammonia, J. Org. Chem. 68 (2003) 1496–1502.

[27] W. Yang, D.G. Drueckhammer, Computational studies of the aminolysis of oxoesters and thioesters in aqueous solution, Org. Lett. 2 (2000) 4133–4136.

[28] T. Shibamoto, R.A. Bernhard, Investigation of pyrazine formation pathways in sugar-ammonia model systems, J. Agric. Food Chem. 25 (1977) 609–614.

[29] F. Glorius, Asymmetric hydrogenation of aromatic compounds, Org. Biomol. Chem. 3 (2005) 4171–4175.

[30] G.B. Baker, R.T. Coutts, A. Holt, Derivatization with acetic anhydride: applications to the analysis of biogenic amines and psychiatric drugs by gas chromatography and mass spectrometry, J. Pharmacol. Toxicol. Methods 31 (1994) 141–148.

[31] J.J. Carberry, The catalytic effectiveness factor under nonisothermal conditions, AlChE J. 7 (1961) 350–351.

[32] G.B. Marin, G.S. Yablonsky, Kinetics of Chemical Reactions: Decoding Complexity, Wiley, New York, 2011.

[33] D.E. Mears, Tests for transport limitations in experimental catalytic reactors, Ind. Eng. Chem. Process Des. Dev. 10 (1971) 541–547.

[34] P.N. Brown, A.C. Hindmarsh, L.R. Petzold, Using Krylov methods in the solution of large-scale differential-algebraic systems, SIAM J. Sci. Comput. 15 (1994) 1467–1488.

[35] J.D. Ramshaw, Fugacity and activity in a nutshell, J. Chem. Educ. 72 (1995) 601.

[36] T. Holderbaum, J. Gmehling, PSRK, a group contribution equation of state based on UNIFAC, Fluid Phase Equilib. 70 (1991) 251–265.

[37] A. Fredenslund, R.L. Jones, J.M. Prausnitz, Group-contribution estimation of activity coefficients in nonideal liquid mixtures, AlChE J. 21 (1975) 1086–1099.

[38] J. Kittrell, Mathematical modeling of chemical reactions, Adv. Chem. Eng. 8 (1970) 97–183.

[39] K. Toch, J.W. Thybaut, G.B. Marin, A systematic methodology for kinetic modeling of chemical reactions applied to *n*-hexane hydroisomerization, AlChE J. 61 (2015) 880–892.

[40] H. Rosenbrock, An automatic method for finding the greatest or least value of a function, Comput. J. 3 (1960) 175–184.

[41] D.W. Marquardt, An algorithm for least-squares estimation of nonlinear parameters, J. Soc. Ind. Appl. Math. 11 (1963) 431–441.

[42] M. Pelckmans, W. Vermandel, F. Van Waes, K. Moonen, B.F. Sels, Low-temperature reductive aminolysis of carbohydrates to diamines and aminoalcohols by heterogeneous catalysis, Angew. Chem. 129 (2017) 14732–14736.

[43] M. Pelckmans, Catalytic Production of Bio-based Amines and Derivatives, Katholieke Universiteit Leuven, 2017.

[44] H. Nursten, The chemistry of nonenzymic browning, the maillard reaction: chemistry, biochemistry and implications, R. Soc. Chem. (2005) 5–30.

[45] S.-L. Zhang, Z.-L. Yu, CC activation by retro-aldol reaction of two β-hydroxy carbonyl compounds: synergy with Pd-catalyzed cross-coupling to access mono-α-arylated ketones and esters, J. Org. Chem. 81 (2016) 57–65.

[46] J. Zhang, B. Hou, A. Wang, Z. Li, H. Wang, T. Zhang, Kinetic study of the competitive hydrogenation of glycolaldehyde and glucose on Ru/C with or without AMT, AlChE J. 61 (2015) 224–238.

[47] R. Ooms, M. Dusselier, J.A. Geboers, B. Op de Beeck, R. Verhaeven, E. Gobechiya, J.A. Martens, A. Redl, B.F. Sels, Conversion of sugars to ethylene glycol with nickel tungsten carbide in a fed-batch reactor: high productivity and reaction network elucidation, Green Chem. 16 (2014) 695–707.

[48] J. Lehtonen, T. Salmi, A. Vuori, E. Tirronen, On the principles of modelling of homogeneous-heterogeneous reactions in the production of fine chemicals. A case study: reductive alkylation of aromatic amines, Org. Process. Res. Dev. 2 (1998) 78–85.

[49] J.S. Campbell, P.H. Emmett, The catalytic hydrogenation of ethylene on nickel-copper and nickel-gold alloys, J. Catal. 7 (1967) 252–262.

[50] D. Roy, R. Jaganathan, R.V. Chaudhari, Kinetic modeling of reductive alkylation of aniline with acetone using Pd/Al2O3 catalyst in a batch slurry reactor, Ind. Eng. Chem. Res. 44 (2005) 5388–5396.

[51] S. Gomez, J.A. Peters, J.C. van der Waal, P.J. van den Brink, T. Maschmeyer, The rationalization of catalyst behaviour in the reductive amination of benzaldehyde with ammonia using a simple computer model, Appl. Catal. A 261 (2004) 119–125.

[52] F. Örsi, Kinetic studies on the thermal decomposition of glucose and fructose, J. Therm. Anal. Calorim. 5 (1973) 329–335.

[53] J. Poissonnier, J.W. Thybaut, G.B. Marin, Large-scale exploitation of bimodal reaction sequences including degradation: comparison of jet loop and trickle bed reactors, Ind. Eng. Chem. Res. (2017).